Steady-State and Time-Resolved Fluorescence Studies on Wild Type and Mutant *Chromatium vinosum* High Potential Iron Proteins: Holo- and Apo-Forms

Apurba K. Sau,* Chun-An Chen,† James A. Cowan,† Shyamalava Mazumdar,* and Samaresh Mitra*
*Department of Chemical Sciences, Tata Institute of Fundamental Research, Colaba, Mumbai 400 005, India and †Evans Laboratory of Chemistry, The Ohio State University, Columbus, Ohio USA

ABSTRACT Detailed circular dichroism (CD), steady-state and time-resolved tryptophan fluorescence studies on the holo- and apo- forms of high potential iron protein (HiPIP) from *Chromatium vinosum* and its mutant protein have been carried out to investigate conformational properties of the protein. CD studies showed that the protein does not have any significant secondary structure elements in the holo- or apo- HiPIP, indicating that the metal cluster does not have any effect on formation of secondary structure in the protein. Steady-state fluorescence quenching studies however, suggested that removal of the iron-sulfur ($[Fe_4S_4]^{3+}$) cluster from the protein leads to an increase in the solvent accessibility of tryptophans, indicating change in the tertiary structure of the protein. CD studies on the holo- and apo- HiPIP also showed that removal of the metal prosthetic group drastically affects the tertiary structure of the protein. Time-resolved fluorescence decay of the wild type protein was fitted to a four-exponentials model and that of the W80N mutant was fitted to a three-exponentials model. The time-resolved fluorescence decay was also analyzed by maximum entropy method (MEM). The results of the MEM analysis agreed with those obtained from discrete exponentials model analysis. Studies on the wild type and mutants helped to assign the fast picosecond lifetime component to the W80 residue, which exhibits fast fluorescence energy transfer to the $[Fe_4S_4]^{3+}$ cluster of the protein. Decay-associated fluorescence spectra of each tryptophan residues were calculated from the time-resolved fluorescence results at different emission wavelengths. The results suggested that W80 is in the hydrophobic core of the protein, but W60 and W76 are partially or completely exposed to the solvent.

INTRODUCTION

Iron-sulfur proteins serve as electron carriers in virtually all living organisms and participate in plant photosynthesis, nitrogen fixation, steroid metabolism, oxidative phosphorylation, and several other processes (Lovenberg, 1973; Spiro, 1982). Proteins containing iron-sulfur clusters have now been identified in a large number of functional contexts, varying from a structural or sensory role in RNA- and DNA-binding and repair proteins or enzymes (Michaels et al., 1990; Prince and Grossman, 1993; Cunningham et al., 1989; Haile et al., 1992; Kennedy et al., 1992; Roulat et al., 1991) to metabolic enzymes (Switzer, 1989), including catalysis of hydrolase isomerization reactions (Chang et al., 1996; Emptage, 1988). It has been reported (Cowan and Lui, 1998) that, for some iron-sulfur proteins where a structural role in a DNA binding protein is suggested, the cluster appears to be nonredox-active. High-potential iron proteins (HiPIPs) comprise a subset of the Fe_4S_4 cluster family of metalloproteins that are characterized by a high positive reduction potential (E_m) in the range of +50 to + 450 mV (Cowan and Lui, 1998). This class is differentiated from the Fe_4S_4 centers in low potential ferredoxins that show negative E_m, typically varying between −100 and −650 mV. The origin of the high reduction potentials of HiPIPs is not yet known. There has been extensive speculation on their involvement in respiratory electron transport chains (Hochkoeppler et al., 1995a,b, 1996; Kerefeld et al., 1996). Support for such a hypothesis has recently emerged from studies of a partially reconstructed reaction center complex from *Rhodoferax fermentans* (Hochkoeppler et al., 1995a,b). In vitro experiments have shown HiPIP to be an electron donor to the *Chromatium* reaction center (Kennel et al., 1972).

HiPIP from *Chromatium vinosum* contains three tryptophan residues (W60, W76, and W80) (see Fig. 1). It also has a tyrosine residue (Y19), which lies in the hydrophobic cluster-binding pocket (Parisini et al., 1999) and plays a critical role in stabilizing the cluster. Both kinetic studies of cluster stability and multinuclear NMR experiments support a model where Tyr^{19} serves to maintain a hydrophobic barrier for exclusion of water from the cluster cavity (Agarwal et al., 1995; Agarwal et al., 1996; Li et al., 1996). The intrinsic fluorescence of the indole moiety of the tryptophan residue is a valuable probe to monitor the conformational properties of the protein (Brand and Johnson, 1997). A combination of steady-state and time-resolved measurements of the protein fluorescence has been useful in obtaining details of the local environment of the protein, its dynamics, and the conformational change associated with the interaction of various molecules.

In the present paper, steady-state and picosecond time-resolved fluorescence studies on wild-type HiPIP, its mutant protein (W80N) and their apo-proteins have been described to understand the conformational changes associ-

Received for publication 20 July 2000 and in final form 10 July 2001.

Address reprint requests to Shyamalava Mazumdar, Department of Chemical Sciences, Tata Institute of Fundamental Research, Homi Bhabha Rd., Colaba, Mumbai 400 005, India. Tel.: +91-22-215-2971; Fax: +91-22-215-2110 or +91-22-215-2181; E-mail: shyamal@tifr.res.in.

0006-3495/01/10/2320/11 $2.00

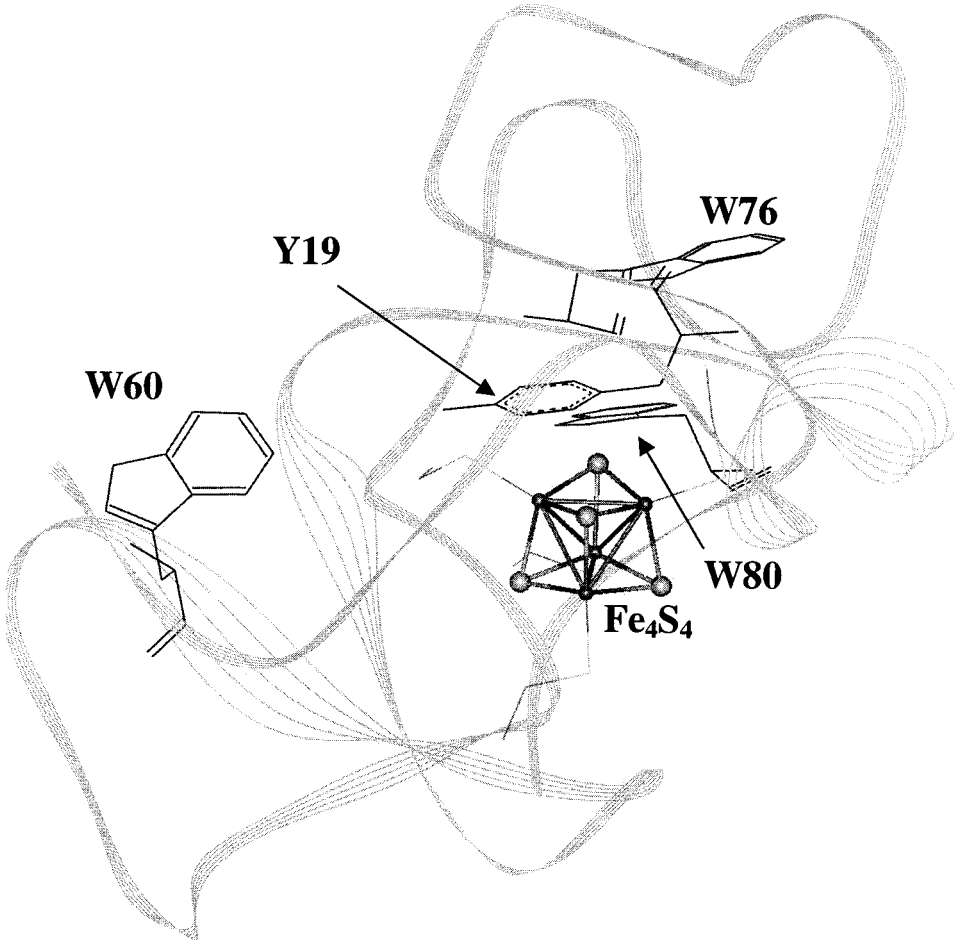

FIGURE 1 Location of the tryptophan residues, the tyrosine residue, and the iron sulfur cluster (shown in ball and stick) of high potential iron protein (HiPIP) from *Chromatium vinosum.* This schematic representation of the protein (monomer unit) was generated from the crystal structure (Protein data bank), accession number 1CKU using the Weblab Viewer program (MSI). The coordinates were obtained from the Protein data bank (Parisini et al., 1999).

ated with mutation and removal of the iron-sulfur cluster. In W80N, tryptophan 80 has been mutated by asparagine.

MATERIALS AND METHODS

Molecular biology and protein chemistry

Protocols for site-directed mutagenesis and characterization of mutant clones have been described elsewhere (Agarwal et al., 1995). Cell cultures were grown, expression induced by IPTG, and initial protein purification was carried out as previously described (Agarwal et al., 1993). Final purification was carried out by FPLC on a Mono Q column (1×5 cm) using nondenaturing condition. Optimal separation of bands was obtained by a gradient method, using two stocks of degassed phosphate buffer, at pH 7.5 (A: 10 mM phosphate and B: 10 mM phosphate, 500 mM NaCl). The total running time was 20 min. (3 min. with 0% B, and 17 min. from 0 to 100% B).

Preparation of Apo-HiPIP

A 15-mg/mL solution of HiPIP in 10 mM NaCl pH 7.5 was diluted with distilled water to a final concentration of 1 mg/mL. A solution of 7.6 M guanidine hydrochloride was added drop wise with stirring to achieve a final concentration of 5 M, and this solution was cooled to 4°C. A solution of 12 N HCl was added to a final concentration of 0.5 N, and the brown or dark green solution immediately turned pink and finally became colorless. This clear solution was agitated under Ar flow for 30 min. and neutralized with concentrated Tris-base solution to pH 7.0. The obtained apo-proteins were exchanged into pH 7.0 distilled water by Amicon ultrafiltration and lyophilized by spin vacuum using a Savant speedvac.

Steady-state fluorescence

Steady-state fluorescence measurements were carried out on a SPEX spectrofluorimeter. The intrinsic fluorescence of the proteins arises from the aromatic amino acid residues such as tryptophan, tyrosine, and phenylalanine. We have used here the fluorescence of the intrinsic tryptophan residues, which are available in the protein under our study. The fluorescence excitation wavelength of 295 nm was used to eliminate the contribution from amino acids other than tryptophan. The emission spectra were recorded from 310 to 500 nm. The monochromator slit width was kept at 5 nm in excitation and emission measurements. The fluorescence measurements of the protein samples were carried out with an optical density of less than 0.1 at 295 nm to avoid the inner filter effect.

The quantum yield for the tryptophan fluorescence of proteins was determined with N-acetyl tryptophanamide (NATA) in water as reference (Das and Mazumdar, 1995a,b). The absolute quantum yields were determined using the reported value of quantum yield of NATA in water as 0.13 (Das and Mazumdar, 1995a,b; Khan et al., 1997).

To understand the solvent accessibility of the tryptophan residues of proteins, tryptophan fluorescence quenching experiments were carried out using three different quenchers; acrylamide (neutral), potassium iodide, and cesium chloride (ionic quenchers). For quenching experiments with potassium iodide, 10 mM sodium thiosulfate buffer was used to prevent the formation of I_3^-. This was necessary because I_3^- also absorbs in the region of tryptophan fluorescence. The Stern–Volmer equation can be used to analyze the quenching of the tryptophan fluorescence:

$$F_0/F = 1 + K_{SV}[Q], \tag{1}$$

where F_0 and F are the fluorescence intensities in the absence and presence of quencher. $[Q]$ is the concentration of the quencher, and K_{SV} is the Stern–Volmer quenching constant. In a protein, which contains several tryptophan residues, the presence of different classes of tryptophan residues (exposed and buried) is reflected in the Stern–Volmer plot. The fraction of total fluorophore accessible to the quencher can be calculated from the modified Stern–Volmer plot, also known as Lehrer plot (Khan et al., 1997).

$$\frac{F_o}{\Delta F} = \frac{1}{K_Q f_a[Q]} + \frac{1}{f_a}, \tag{2}$$

where F_0 is same as defined earlier and ΔF is the change in the fluorescence intensity due to quenching, K_Q is the Stern–Volmer quenching constant of the exposed tryptophan residues and f_a is the fraction of the initial fluorescence, which is accessible to the quencher. F_0 and $[Q]$ have the same meaning as above.

Time-resolved fluorescence spectroscopy

The time-resolved tryptophan fluorescence studies were carried out using a tunable dye-laser pulse from a synchronously pumped cavity-dumped dye laser (Rhodamine 6G) driven by frequency-doubled output (532 nm) of the CW mode-locked Nd-YAG laser system described elsewhere (Das and Mazumdar, 1995ab). Fluorescence decay profiles were collected using a time-correlated single photon counting device coupled to microchannel plate photomultiplier. The width of the dye laser pulse was typically 4–6 ps and the half-width of the instrument response function was frequency doubled to generate the ultraviolet beam at 295 nm, which was used to excite the samples. The instrument response functions were obtained from a purely scattering medium. Emission profiles were collected at the magic angle (54.7°) of emission polarizer to avoid any contribution from anisotropy. A Schott WG 320 cutoff filter was used before the monochromator to remove any scattering from samples at wavelengths below 320 nm. To get the fluorescence decay curves, $1–2 \times 10^4$ counts were collected in the peak channel (total counts, $7–12 \times 10^5$). Each data set was collected in 512 channels, and the width was 37.84 or 75.68 ps. Protein samples were used in 100 mM sodium phosphate buffer, pH 7.0 for the time-resolved fluorescence measurements. The apparatus response was always checked by measuring the lifetime of N-acetyl tryptophanamide (NATA) as a standard before starting the accumulation of data for the protein samples.

The observed fluorescence decay data, $[F(t)]$, is a convolution of the instrument response function $[R(t)]$, and the intensity of fluorescence decay function $[I(t)]$ of the sample,

$$F(t) = \int_0^i R(s + \delta)I(t - s)\mathrm{d}s, \tag{3}$$

where δ is the shift parameter, which is a fraction of the time/channel; $R(t)$ is experimentally determined, and $I(t)$ is a function assumed to describe the fluorescence dynamics of the sample. The analysis of the data involves the determination of the best values for the parameters in $I(t)$.

The fluorescence decay was fitted to a function that is a sum of discrete exponentials,

$$I(t) = \sum_i \alpha_i \exp(-t/\tau_i), \quad i = 1 - n \tag{4}$$

where α_i and τ_i are the amplitude and fluorescence lifetime for the ith component. To determine the amplitudes and lifetimes, an iterative reconvolution was applied using nonlinear least square regression by Marquardt's algorithm for parameter optimization (Das and Mazumdar, 1995a,b). The validity of the exponential fit was always checked by many cycles of iteration. The goodness of the exponential fit was determined from the random residual distribution with a χ^2 value close to unity.

Analysis of the fluorescence decay profiles was also carried out by the maximum entropy method (MEM) using a uniform distribution of the lifetime components in a logarithmic time scale. This method is based on choosing a distribution of amplitudes, α_i that yields maximum value of the entropy, S (also called Shannon–Jaynes entropy) at the optimized χ^2, which is defined as (Das and Mazumdar, 1995ab; Khan et al., 1997).

$$S = -\int \alpha(\tau)\log\frac{\alpha(\tau)}{m(\tau)}\,\mathrm{d}\tau \tag{5}$$

where the starting model, $m(\tau)$, is a flat distribution of amplitudes in the log τ scale. Maximization of the entropy function, S, was carried out under χ^2 constraint defined as

$$\chi^2 = \frac{1}{M}\sum_{m=1}^{M}\frac{[F_{cal}^m(t) - F_{exp}^m(t)]^2}{\sigma_m^2} \approx 1.0, \tag{6}$$

where $F_{cal}^m(t)$ and $F_{exp}^m(t)$are the calculated and observed intensities respectively at time t, σ_m^2 is the variance of the mth channel, and M is the number of the data points (total number of channels). Here, the fluorescence intensity can be defined as

$$F(t) = R(t) \otimes \int \alpha(\tau)\exp(-t/\tau)\,\mathrm{d}\tau \tag{7}$$

where $R(t)$ is the temporal shape of the excitation pulse, and $\otimes$ denotes a convolution product. The optimized amplitude distribution α_i recovered by MEM represents the maximum probable distribution of amplitudes along the lifetime components. The final outputs of MEM analysis were displayed as amplitude distribution of lifetime components in a logarithmic scale.

Decay-associated spectra

The decay-associated emission spectra (DAS) of tryptophan fluorescence of proteins were constructed from the steady-state spectra and the time-resolved fluorescence decay parameters $\alpha_i(\lambda)$ and $\tau_i(\lambda)$ at different wavelength (Das and Mazumdar,1995a,b; Khan et al., 1997). The intensity $I_i(\lambda)$ due to the ith component at particular wavelength λ, can be written as

$$I_i(\lambda) = I(\lambda)\frac{\alpha_i(\lambda)\tau_i(\lambda)}{\Sigma_i\,\alpha_i(\lambda)\tau_i(\lambda)}, \tag{8}$$

where $I(\lambda)$ is the total fluorescence intensity obtained from the steady fluorescence emission spectra, $\alpha_i(\lambda)$ and $\tau_i(\lambda)$ are the amplitude and lifetime of ith component at wavelength λ. Hence, $I(\lambda)$ multiplied by the fractional contribution $\alpha_i(\lambda)\tau_i(\lambda)/\Sigma_i\,\alpha_i(\lambda)\tau_i(\lambda)$ will give the individual con-

tribution to the steady-state intensity due to each component at a particular wavelength λ. The decay profiles were obtained at a particular wavelength in the wavelength range of the steady-state spectra.

Fluorescence-energy transfer

The major mechanism of the decrease in fluorescence lifetimes in heme proteins arises from energy transfer to the heme group (Khan et al., 1997; Hochstrasser and Negus, 1984). In iron-sulfur proteins, the decrease in tryptophan fluorescence lifetime is due to energy transfer from tryptophan residues to the iron-sulfur cluster. Förster's theory of resonance-energy transfer can be used to estimate the distance of the fluorophore from the acceptor group (Khan et al., 1997; Hochstrasser and Negus, 1984; Beechem and Brand, 1985). The efficiency of energy transfer, *E*, from the donor to the acceptor group is given by Förster's theory,

$$E = 1 - \tau_{da}/\tau_{d}\,, \tag{9}$$

where τ_{da} and τ_{d} represent the lifetime values of the fluorophore in the presence and absence of the acceptor group, respectively. The energy-transfer efficiency (*E*) is related to the distance, *R*, between the centers of the fluorophore and the acceptor by the equation (Hochstrasser and Negus, 1984; Beechem and Brand, 1985),

$$E = \frac{R_0^6}{R^6 + R_0^6}\,, \tag{10}$$

where R_0 is the distance at which the energy-transfer efficiency is 50%. R_0 is defined by the equation,

$$R_0 = (J\kappa^2 Q_d n^{-4})^{1/6} \times 9.79 \times 10^2 \text{ nm}, \tag{11}$$

where *J* is spectral overlap integral; κ^2 is the orientation factor for the dipole–dipole interaction, *n* is the refractive index of the medium separating the donor and acceptor groups and was taken to be 1.4, and Q_d is the quantum yield of the donor in the absence of acceptor. The value of the overlap integral (Hochstrasser and Negus, 1984) between the donor emission and acceptor absorption is given by the equation,

$$J = \frac{\int F(\lambda)\epsilon(\lambda)\lambda^4\, d\lambda}{\int F(\lambda)\, d\lambda} \tag{12}$$

where $F(\lambda)$ and $\epsilon(\lambda)$ are the observed fluorescence intensity of the donor and the absorption coefficient ($cm^{-1}M^{-1}$) of the acceptor at a wavelength λ, respectively. The value of *J* was determined numerically (Das and Mazumdar, 1995a,b; Khan et al., 1997) over the region 310–500 nm for tryptophan emission.

One of the important factors that determine the efficiency of energy transfer is the relative orientation of the transition dipoles of the donor and acceptors in space, described above as κ^2. Depending upon the relative orientation of donor and acceptor, this factor can range from 0 to 4. For parallel alignment of the transition dipoles, $\kappa^2 = 4$ and if the dipoles are oriented perpendicular to one another, $\kappa^2 = 0$.

Electronic absorption and CD studies

Electronic absorption spectral studies of HiPIP were carried out using a Shimadzu UV2100 spectrophotometer attached to an IBM PC-486. Concentrations of the proteins were determined by reported methods (Przysiecki et al. 1985; Kulzer et al., 1998) using $\epsilon_{388} = 16.1\ mM^{-1}\ cm^{-1}$ for the holo-HiPIP and $\epsilon_{280} = 11.8\ mM^{-1}\ cm^{-1}$ for the apo-protein. Circular dichroism studies were carried out using a Jasco J-600 spectropolarimeter (Chattopadhyay and Mazumdar, 2000). All experiments were carried out at room temperature, i.e., 25°C.

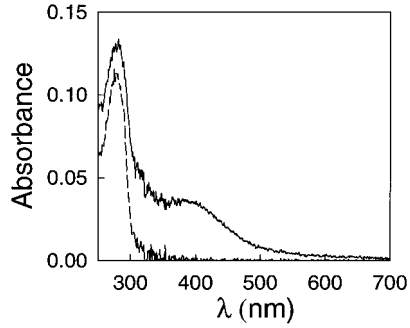

FIGURE 2 Optical spectra of wild-type HiPIP (*solid line*) and its apo-protein (*dashed line*) in 100 mM NaH_2PO_4 at pH 7.0. The concentrations of the proteins were 2.5 and 9.3 μM, respectively.

RESULTS AND DISCUSSION

Electronic absorption spectra

Figure 2 shows the optical spectra of wild-type HiPIP and its apo-protein. Upon removal of the $[Fe_4S_4]^{3+}$ cluster from the wild-type protein, the optical band at 398 nm disappears, indicating that the band is due to the $[Fe_4S_4]^{3+}$ cluster. The optical spectra for the mutant W80N and its apo-proteins were similar (data not shown).

CD spectra

Figure 3 shows the CD spectra of the wild-type HiPIP and its apo-protein. Complete absence of the CD of the apo-HiPIP in the visible region (300–600 nm) showed that the CD in this region originates from the transitions in the $[Fe_4S_4]^{3+}$ cluster (Fig. 3 *A*). The magnitudes of the mean residue molar ellipticity ([Θ]) for the holo- and the apo-HiPIP in the protein region (190–260 nm) are very small, which indicated that the protein has very little secondary structure both in the holo- and apo- forms (Fig. 3 *B*). Analysis of the CD spectra in the far UV region by neural network method using CDNN program (Bohm et al., 1992) showed that there is <10% helicity in the protein and practically no change in the helicity was observed between the holo- and the apo-protein (Table 1). The CD spectra of the holo-protein matched with earlier report (Przysiecki et al. 1985). The bands near 230 and 200 nm (Fig. 3 *B*) have earlier been shown (Przysiecki et al. 1985; Brahms and Brahms, 1980) to arise due to tertiary interactions and contributions from the $[Fe_4S_4]^{3+}$ cluster, which become predominant in the holo-HiPIP. Removal of the $[Fe_4S_4]^{3+}$ cluster thus does not have any effect on the secondary structure of the protein but causes change in the tertiary structure of the protein, which gives rise to the differences observed in the CD spectra of the holo- and apo-HiPIP in the protein region. The crystal structure of the protein (Fig. 1) also shows very little helical structure in the protein, which agreed with the CD results. NMR studies of apo-

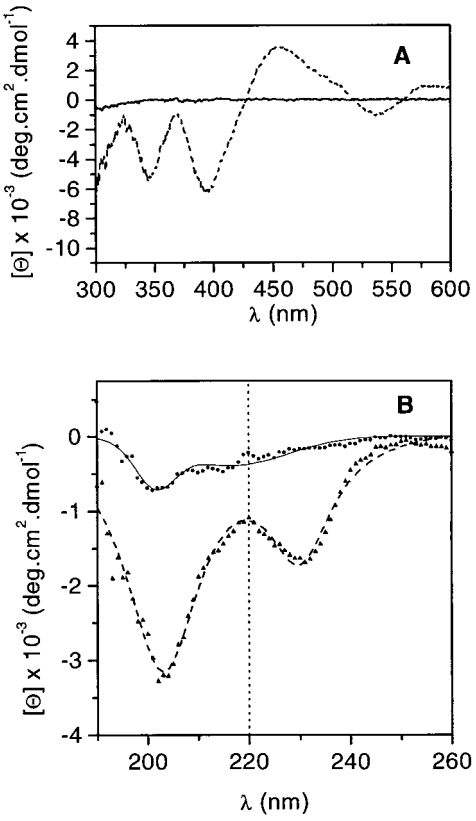

FIGURE 3 Circular Dichroism spectra of holo- (*dashed lines*) and apo- (*solid lines*) HiPIP in 100 mM NaH_2PO_4 at pH 7.0, in (*A*) visible region (300–600 nm), and (*B*) protein region (190–260 nm). The CD in the protein region is expressed as mean residue ellipticity whereas that in the visible region is expressed as molar ellipticity.

HiPIP and holo-HiPIP have recently been reported (Natarajan and Cowan, 1997), which showed that the tertiary structure of the holo-protein was formed on gradual incorporation of iron forming the $[Fe_4S_4]^{3+}$ cluster in the protein. The results thus indicate that, although both the apo- and holo-HiPIP do not have any secondary structure, but different segments of the apo-protein might come close together to form a compact tertiary structure in the holo-protein on incorporation of the metal cluster. Removal of the $[Fe_4S_4]^{3+}$ cluster from the holo-protein thus breaks the tertiary structure of the protein.

TABLE 1 Analysis of the circular dichroism spectra of the holo- and apo-proteins of wild-type HiPIP and W80N HiPIP

Protein	Helix (%)	Anti-Parallel (%)	Parallel (%)	Beta-turn (%)	Random coil (%)
Wild-type HiPIP	4.6	39.3	5.0	18.1	33.0
Apo-HiPIP	3.6	41.7	4.8	17.6	32.3
W80N HiPIP	5.0	39.5	5.1	17.9	32.5
Apo-W80N HiPIP	4.7	37.0	5.1	17.4	35.8

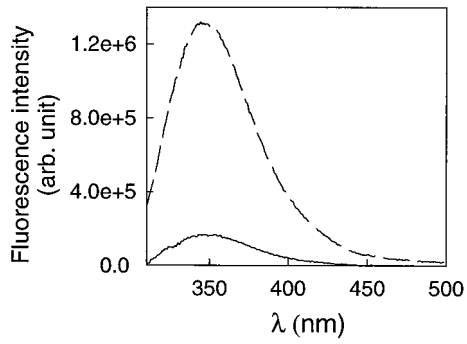

FIGURE 4 Steady-state fluorescence emission spectra of wild-type HiPIP (*solid line*) and its apo-protein (*dashed line*) in 0.1 M sodium phosphate buffer at pH 7.0. The concentrations of the wild-type HiPIP and its apo-protein were 8.7 and 16.1 μM, respectively. The excitation wavelength was 295 nm.

Steady-state fluorescence

Fluorescence emission spectra

The fluorescence emission spectra of wild-type HiPIP and W80N-HiPIP showed a broad band at 347 nm, whereas, for their apo-proteins, a band around 352 nm was observed (see Fig. 4). This agrees with the reported fluorescence spectra of HiPIP (Bian and Cowan, 1998). The position of the tryptophan fluorescence emission spectrum is indicative of the nature of the environment and the dielectric constant of the medium around it. The steady-state fluorescence emission spectrum of NATA shows a fluorescence emission band at 360 nm in 100 mM phosphate buffer, pH 7.0. The observed emission maxima of wild type HiPIP and their mutant proteins at 347 nm thus indicate that the average environment of the tryptophan residues is relatively polar. However, the bands for the apo-proteins show red shift compared to their native form, suggesting that the removal of $[Fe_4S_4]^{3+}$ cluster increases the polarity of the environment of tryptophan residues.

The steady-state quantum yields of wild-type HiPIP, its mutant, and their apo-proteins were determined using NATA in 100 mM phosphate buffer, pH 7.0 as reference and are listed in Table 2. The low quantum yields of native and mutant proteins compared to their apo-proteins suggest that there is an efficient energy transfer from the tryptophan

TABLE 2 Quantum yield (with respect to NATA) of the protein and percentage of tryptophan residues accessible to the solvent

Protein	Quantum Yield	% of Tryptophan residues accessible to solvent
Wild-type HiPIP	0.002	60
Apo-HiPIP	0.022	75
W80N HiPIP	0.007	75
Apo-W80N HiPIP	0.020	85

residues to the iron-sulfur cluster. The low quantum yield of the tryptophan fluorescence has also been found in several heme proteins due to efficient energy transfer from the tryptophan residues to the heme group (Hochstrasser and Negus, 1984).

Steady-state fluorescence quenching

The quenching of fluorescence requires the molecular contact between the quencher and the fluorophore in either ground or excited states, and can therefore be used to determine the surface accessibility of the tryptophan resides by using different quenchers. Acrylamide, a neutral and efficient quencher is known to quench the fluorescence of tryptophan residues exposed to the solvent and buried in the protein. However, potassium iodide and cesium chloride, positively and negatively charged quenchers, respectively, could quench only those tryptophan residues, which are exposed to the solvent but not the ones buried inside the protein. Fluorescence quenching studies can therefore give information on the number of tryptophan residues exposed to the solvent.

The fluorescence intensities of the holo and apo-proteins of HiPIP were found to decrease on addition of the quenchers. The decrease in the fluorescence intensity was much smaller for KI or CsCl than for acrylamide. The nature of the Stern–Volmer plot for acrylamide is linear, indicating that all the tryptophan residues are accessible to acrylamide (Fig. 5*A*). This is further confirmed from the Lehrer's plot (Fig. 5 *B*), which is linear with intercept ~1. However, the Stern–Volmer plots for KI and CsCl show downward curvature (Fig. 5 *A*) at higher concentrations of the quenchers, indicating that only part of the tryptophan residues is accessible to these ionic quenchers. The percentage of the total fluorescence quenched by these ionic quenchers was calculated using Eq. 2 from the Lehrer's plot (Fig. 5 *B*) and found to be ~60%. The fluorescence quenching of apo-HiPIP by the quenchers was carried out to investigate whether there was any change in the environment of the tryptophan residues on removal of iron-sulfur cluster from the holo-protein. The Lehrer plot for acrylamide is linear with intercept ~1, indicating that all the tryptophan residues in the apo-protein are also accessible to acrylamide (data not shown). However, the percentage of total fluorescence quenched by KI and CsCl from Lehrer plot was found to be ~75% in apo-HiPIP. The removal of the iron-sulfur cluster in apo-HiPIP thus slightly increases the solvent accessibility of the tryptophan compared to the holo-protein.

The data of the fluorescence quenching experiments on W80N HiPIP and its apo-protein with these quenchers were similarly analyzed. The results obtained from the Lehrer's plot are included in Table 2 and show that the solvent accessibility of the tryptophan residues of W80N protein is more than the native protein. As in wild-type HiPIP, the removal of the $[Fe_4S_4]^{3+}$ cluster increases the solvent accessibility of the tryptophan.

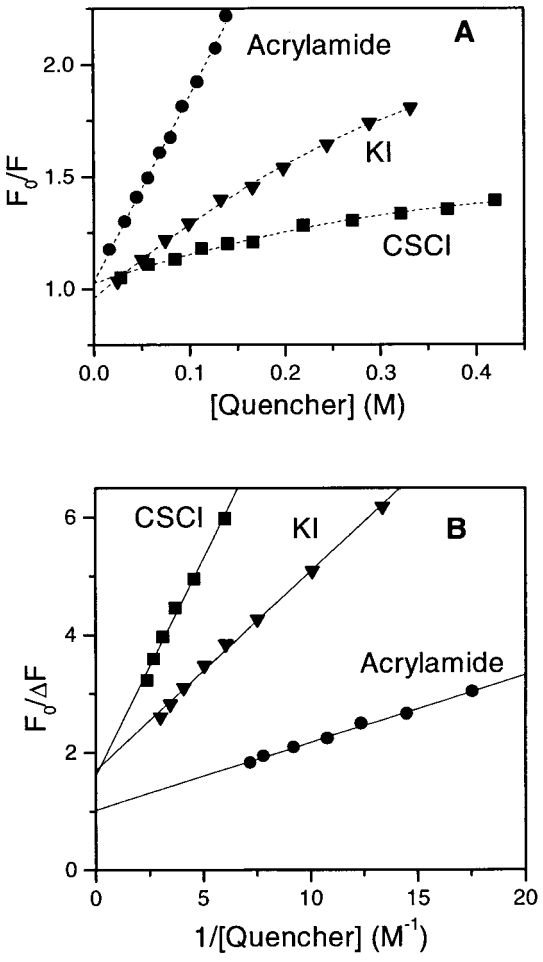

FIGURE 5 (*A*) Stern–Volmer plots for the tryptophan fluorescence quenching of wild-type HiPIP by three quenchers: acrylamide, KI, and CsCl. (*B*) Lehrer plots for the same set of data.

Time-resolved fluorescence

Fluorescence decay curve

The time-resolved fluorescence decay curve of wild-type HiPIP protein is shown in Fig. 6*A*. Attempts to fit the data to one, two, or three exponential models were found to be inadequate, and the data fitted best to a four-exponential model. The goodness of the fit was judged by the random residuals distribution, autocorrelation function and χ^2 minimization criteria (χ^2 was kept in the range of 1.0–1.2). The fluorescence lifetimes obtained from the exponential analysis were $\tau_1 = 0.04$ ns, $\tau_2 = 0.5$ ns, $\tau_3 = 2.1$ ns, and $\tau_4 = 5.4$ ns. The amplitudes of these lifetimes were found to be $\alpha_1 = 75\%$, $\alpha_2 = 13\%$, $\alpha_3 = 10\%$ and $\alpha_4 = 2\%$ respectively.

The analysis of the fluorescence decay curve was also carried out by the maximum entropy method (MEM). The

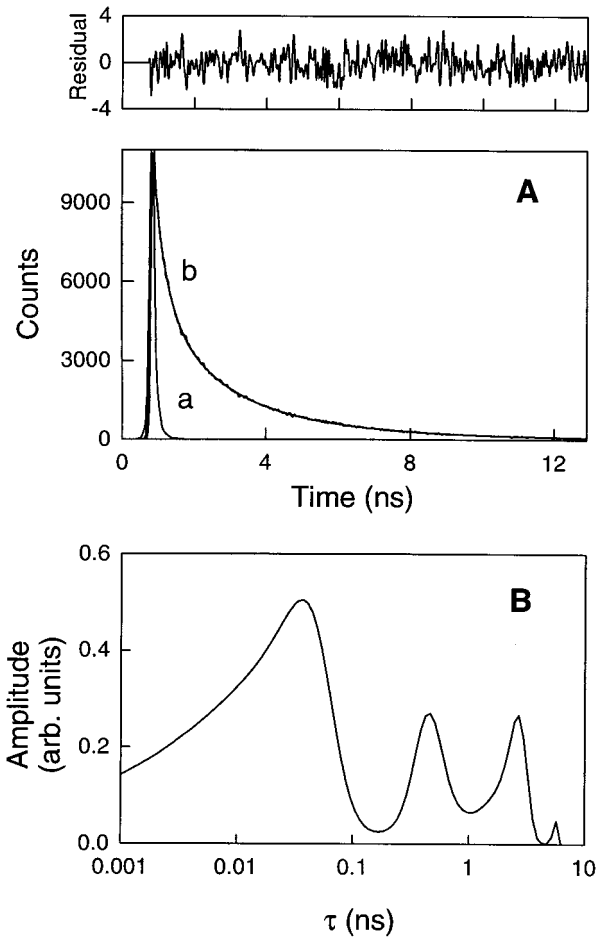

FIGURE 6 (*A*) Time-resolved fluorescence decay of (*a*) wild-type HiPIP and (*b*) the instrument response function. The solid line drawn through the decay curve shows a four-exponential fit to Eq. 4 with $n = 4$. The upper curve shows the random residual distribution $[F_{cal}(t) - F_{exp}(t)]$ plot showing the accuracy of the exponential fit. (*B*) Amplitude distribution of tryptophan fluorescence lifetimes for wild-type HiPIP recovered from MEM analysis.

MEM analysis of fluorescence decay data assumes that all possible lifetimes in a given range of 10 ps to 10 ns have equal probability. The initial assumed distribution plot of probability or amplitude versus lifetime is flat and the analysis starts from the unbiased distribution of the lifetimes. The MEM analysis of the wild-type protein shows four classes of lifetime distributions with bericenters around 0.04, 0.5, 2.2, and 5.4 ns (Fig. 6 *B*). The values of the mean lifetimes obtained by the MEM analysis agreed very well with the discrete exponential analysis method.

The time-resolved fluorescence decay curves for apo-HiPIP were similarly obtained and the data were analyzed by the discrete exponential and MEM analysis methods. The data were best fitted to a four exponential model with lifetimes of 0.14, 0.5, 1.8 and 5.5 ns. The corresponding amplitudes of these lifetimes were found to be 54%, 28%, 16%, and 2%, respectively. The fluorescence decay of the mutant W80N-HiPIP and its apo-protein were obtained and the data were similarly analyzed. The fluorescence decay for W80N-HiPIP and its apo-protein was best fitted to a three-exponential model. The lifetimes and their amplitudes are listed in Table 3.

The fluorescence decay for tryptophan residue is known to be multiexponential in single and in multiple tryptophan-containing proteins (Das and Mazumdar, 1995a,b; Khan et al., 1997; Hochstrasser and Negus, 1984; Beechem and Brand, 1985; Robbins et al., 1985). The multiexponential decay may arise due to the conformational isomers in the ground state of tryptophan residue, where the local environment of the indole chromophore differs substantially. The time-resolved fluorescence decay of the wild-type HiPIP and its apo-protein show four lifetimes obtained by discrete exponential and MEM analysis method. The choice of a four exponential model is adequate as judged by the random residual distribution and the χ^2-minimization criteria.

The decrease in τ_1 of HiPIP compared to its apo-protein is due to fluorescence resonance energy transfer between the tryptophan residue and the iron-sulfur cluster, which is absent in the apo-protein. The absence of the shortest lifetime component (τ_1) in W80N-HiPIP indicates that τ_1 of HiPIP possibly arises solely from the W80 tryptophan residue. It has been observed that fluorescence lifetimes of different tryptophan residues in heme proteins generally lie in the picosecond range due to very efficient electron transfer from the excited state of tryptophan to the heme (Beechem and Brand, 1985, Das and Mazumdar, 1995b). The low value of τ_1 in wild-type HiPIP is therefore not surprising. The other three lifetime components of the protein possibly arise from the tryptophan residues W76 and W60, which are far away from the iron-sulfur cluster and less efficient in the energy transfer to the cluster.

Table 3 shows that the average lifetimes (τ_m) for the holo-proteins are larger than those of the apo-proteins. Moreover, the values of τ_m for the wild type protein are smaller than those for the W80N mutant, whereas their observed quantum yields are almost similar to each other. Removal of the metal cluster from the holo-protein causes a drastic change in the tertiary structure of the protein as discussed in the previous section, which may significantly affect the solvent environment (e.g., polarity) of the tryptophans lying far from the metal cluster. Such changes in the tertiary structure might thus lead to decrease in one or more long-lifetime components (e.g., τ_3 in Table 3) in the apo-HiPIP compared to the holo-protein, causing an apparent decrease in the average lifetime of the apo-protein. Mutation of the W80 residue (i.e., in W80N) leads to complete absence of the fast-lifetime component (τ_1). The remaining two tryptophans (W76 and W60) in the mutant protein do not show appreciable energy transfer to the iron-sulfur cluster, which possibly leads to an apparent increase in the average lifetime of the mutant protein. The observed steady-

TABLE 3 Fluorescence decay parameters recovered by exponential analysis

Protein	$\tau_1(\alpha_1)$ (ns)	$\tau_2(\alpha_2)$ (ns)	$\tau_3(\alpha_3)$ (ns)	$\tau_4(\alpha_4)$ (ns)	τ_m* (ns)
Wild-type HiPIP	0.04 ± 0.01 (0.754)	0.5 ± 0.1 (0.128)	2.1 ± 0.2 (0.103)	5.4 ± 0.3 (0.014)	2.3 ± 0.1
Apo-HiPIP	0.14 ± 0.01 (0.543)	0.5 ± 0.1 (0.278)	1.8 ± 0.2 (0.164)	5.5 ± 0.3 (0.015)	1.8 ± 0.1
W80N HiPIP	—	0.4 ± 0.1 (0.370)	2.1 ± 0.2 (0.424)	5.6 ± 0.3 (0.207)	3.8 ± 0.1
Apo-W80N HiPIP	—	0.5 ± 0.1 (0.550)	1.9 ± 0.2 (0.364)	5.7 ± 0.3 (0.080)	2.8 ± 0.1

*$\tau_m = \Sigma(\alpha_i\tau_i^2)/\Sigma(\alpha_i\tau_i)$.

state fluorescence of the holo- and apo-protein would possibly have very little contribution from the fast-lifetime component (e.g., W80 residue in holo-protein, see below). Hence the observed steady-state fluorescence intensity (Fig. 4) and quantum yields (Table 2) for the holo-proteins of the wild-type and W80N mutant are much smaller compared to the apo-proteins. The fluorescence decay of the W80N mutant is dominated by the longer lifetime components (τ_2, τ_3, τ_4), hence the average lifetime of the mutant is larger than that of the wild-type protein.

Decay-associated spectra

DAS were computed from the steady-state fluorescence emission spectra and the wavelength dependence of the time-resolved fluorescence decay of the proteins (Khan et al., 1997; Robbins et al., 1985; Das and Mazumdar, 1995a,b). The fluorescence decay profiles with excitation at 295 nm and emission at wavelengths ranging from 315 to 400 nm were analyzed by discrete exponentials and by global analysis methods. The lifetimes obtained by discrete exponential analysis at different wavelengths were found to show only a small variation with wavelength. This type of variation of lifetime components has also been observed in previous reports and possibly arises from differences in experimental conditions and instrument responses (Robbins et al., 1985; Das and Mazumdar, 1995a,b; Godik et al., 1993). To obtain the decay-associated spectra, global analysis of the fluorescence decay was carried out to produce optimized values of lifetimes consistent with all experimental data. The values of lifetimes obtained by global analysis of the decay profile at different emission wavelengths were found to be close to those obtained at 347 and 352 nm for the native and their apo-proteins, respectively. The pre-exponential factors from the time-resolved data were used to construct the decay-associated emission spectra using Eq. 8. Figure 7*A* shows the DAS for the wild-type HiPIP, calculated from the four exponentials model, and solid lines show the Gaussian fits to the spectra. The values of λ_{max} corresponding to the lifetime components obtained by the Gaussian fits to the decay-associated spectra are given in Table 4. Table 4 shows that the DAS of the tryptophan residue corresponding to the lifetime component τ_1 is blue shifted (λ_{max} = 320 nm) compared to those of the other lifetime components. Based on our data, we have assigned τ_1 of wild-type HiPIP to the W80 residue. W80 is therefore expected to lie much deeper in the hydrophobic core of the protein than the other tryptophan residues. The lifetime components τ_2, τ_3, and τ_4 may originate from either or both W76 and W60 residues. We have also studied the wavelength dependence of fluorescence emission dynamics for W80N-HiPIP and its apo-protein, and the decay-associated spectra were similarly constructed.

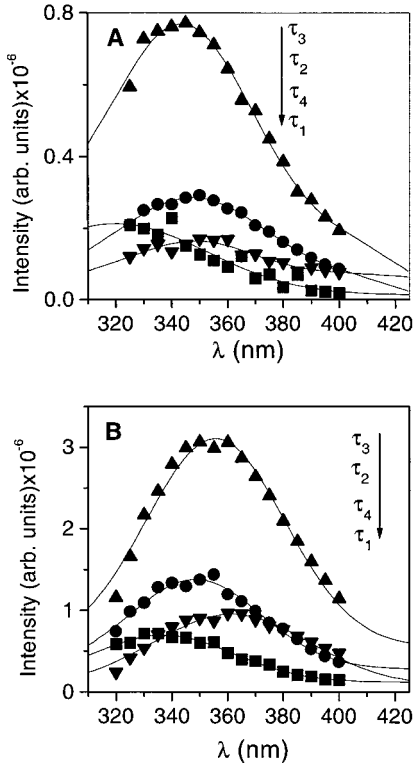

FIGURE 7 Decay-associated emission spectra of the lifetime components, as calculated from Eq. 8, of (*A*) wild-type HiPIP and (*B*) apo-HiPIP obtained from the four-exponential global fit to the time-resolved fluorescence decay data. The solid lines show Gaussian fits to the data.

TABLE 4 Fluorescence emission maxima (λ_{max}) obtained from the decay-associated spectra

Protein	λ_{max} (τ_1) (nm)	λ_{max} (τ_2) (nm)	λ_{max} (τ_3) (nm)	λ_{max} (τ_4) (nm)
Wild-type HiPIP	320	347	343	348
Apo-HiPIP	337	348	355	361
W80N HiPIP	—	347	342	349
Apo-W80N HiPIP	—	348	353	359

The DAS analysis indicated that the overall steady-state spectrum of the protein would have lesser contribution from the W80 residue than that from other tryptophan residues. The quantum yield is proportional to the area of the emission band of the fluorophor. The DAS analysis showed that the area of the DAS corresponding to τ_1 is ~20% of the total area of the steady-state emission of the protein, indicating that the W80 residue would have lower quantum yield compared to the other two residues. Assuming that the fluorescence quantum yields of W76 and W60 were equal, one could estimate that the observed (60%) solvent accessibility of tryptophan fluorescence (see Table 2) in the holo-HiPIP corresponds to ~1.5 tryptophans exposed to the solvent. This result agrees with the quenching results of the W80N mutant of HiPIP (Table 2). Similar assignment of lifetimes could not be made in case of the apo-proteins, and the emission maxima of all the lifetime components in DAS of the apo-HiPIP are red shifted compared to the holo-proteins (Fig. 7 *B*, Table 4). This indicated that there might be change in the tertiary structure of the protein so that the tryptophan residues possibly move toward the solvent upon removal of the $[Fe_4S_4]^{3+}$ cluster from the HiPIP. This result agrees with the circular dichroism (Table 1) and with the steady-state fluorescence quenching (Table 2) studies described in the previous section.

Fluorescence energy transfer

The spectral overlap integral (J), determined numerically over the region 310–500 nm for tryptophan emission, were found to be 1.09×10^{-15} and 8.6×10^{-16} $cm^3\,M^{-1}$ at pH 7.0 for the wild-type HiPIP and W80N HiPIP, respectively. The efficiency of energy transfer from tryptophan to the iron-sulfur cluster depends on the distance and the relative orientation of the cluster and tryptophan residue, and it was calculated using Eq. 9. The relative orientation of the two choromophores is expressed by a quantity called κ^2 (orientation factor). The distances of the tryptophan residues from the core of the iron-sulfur cluster were determined from the x-ray crystallographic data (PDB code 1CKU, Parisini et al., 1999) using the Biosym program (Mol. Sim. Inc.), and were found to be 7.5 Å (W80), 10 Å (W76) and 14 Å (W60), which are shown as horizontal lines in Fig. 8. The values of calculated distances (R_{cal}) were determined from Eqs. 10–11 for all values of κ^2 (in the range 0–4) using the

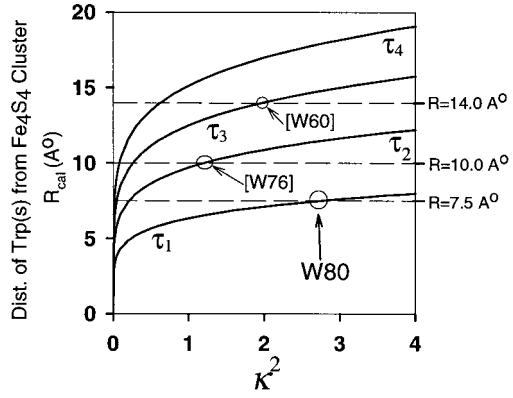

FIGURE 8 Plot of κ^2 against the distance of tryptophan residue from the iron-sulfur cluster. The dotted line shows the crystallographic distance for the tryptophan residues W80, W76, and W60. The solid lines labeled τ_1, τ_2, τ_3, and τ_4 show the calculated distances of the iron-sulfur cluster from the tryptophan residues, determined from fluorescence energy transfer using all possible values of κ^2 (0.0–4.0). The point of intersection between the crystallographic distance line and calculated distance curve shows the value of κ^2 for the tryptophan residue assigned to the lifetime.

experimentally observed values of τ_1, τ_2, τ_3, and τ_4. Figure 8 shows plots of the calculated distances (R_{cal}) between the tryptophan residue and the $Fe_4S_4{}^{3+}$ cluster against κ^2 for each lifetime component. The intersection of a calculated distance curve and the horizontal line of crystallographic distance would give the estimated value of the orientation factor, κ^2 expected for the corresponding tryptophan residue. The fastest lifetime component, τ_1 in HiPIP, as discussed in the previous section, was assigned to arise solely due to fast energy transfer from the W80 to the iron-sulfur cluster; whereas assignment of other lifetime components were ambiguous. The value of κ^2 was found to be ~2.8 (see the intersection of the two lines in Fig. 8, labeled W80) for W80 residue. The κ^2, so determined, was found to agree well with the known crystallographic disposition of W80 with respect to the iron-sulfur cluster. Figure 8 also shows the calculated distance plots for other tryptophan residues and tentative assignments of their lifetimes (labeled as W76 and W60 at the intersection points). However, as mentioned above, W76 and W60 residues may also have multiple lifetimes (as indicated by DAS analysis) hence the assignment of a single lifetime to them may be ambiguous (hence the assignments are shown in brackets).

CONCLUSIONS

Steady-state and time-resolved fluorescence studies on wild-type HiPIP, its mutant, and their apo-proteins have been carried out to investigate the structural properties of the protein in the holo- and apo- forms. Steady-state quenching results show that the solvent accessibility of the tryptophans increases upon removal of the iron-sulfur cluster from the native and mutant proteins. The time-resolved

fluorescence results on the wild-type HiPIP showed that the fluorescence decay is dominated by a picosecond-lifetime component ($\tau_1 \approx 40$ ps), which arises due to fast energy transfer from tryptophan to the iron-sulfur cluster. The lifetime component τ_1 of wild-type HiPIP was found to arise solely from W80. Apo-HiPIP shows an enhancement of τ_1 upon removal of the iron-sulfur cluster. Decay-associated spectra suggested that W80 is in the hydrophobic core of the protein, but W60 and W76 are partially or completely exposed to the solvent.

A comparison of the results of wild-type HiPIP and W80N HiPIP brings out a special feature of the tryptophan fluorescence in the iron sulfur proteins. The absence of the Trp^{80} in the W80N HiPIP results in complete absence of the fast picosecond-lifetime component in the tryptophan fluorescence decay of the mutant protein. The wild-type protein follows four exponentials fluorescence decay, whereas the mutant protein shows three exponentials decay of the tryptophan fluorescence.

Authors wish to thank Mr. Bharat T. Kansara and Dr. Gong Wu for help. The work was supported by the Tata Institute of Fundamental Research.

REFERENCES

Agarwal, A., J. Tau, M. Eren, A. Tevelev, S. M. Lui, and J. A. Cowan. 1993. Synthesis, cloning and expression of a synthetic gene for high potential iron protein from *Chromatium vinosum. Biochem. Biophys. Res. Commun.* 197:1357–1362.

Agarwal, A., D. Li, and J. A. Cowan. 1995. Role of aromatic residues in stabilization of the $[Fe_4S_4]$ cluster in high-potential iron proteins (HiPIPs): physical characterization and stability studies of Tyr-19 mutants of *Chromatium vinosum* HiPIP. *Proc. Natl. Acad. Sci. U.S.A.* 92:9440–9444.

Agarwal, A., D. Li, and J. A. Cowan. 1996. Influence of oxygen ligation on $[Fe_4S_4]$ cluster properties: Characterization of the Cys77Ser mutant of *Chromatium vinosum* HiPIP. *J. Am. Chem. Soc.* 118:927–928.

Beechem, J. M., and L. Brand. 1985. Time-resolved fluorescence of proteins. *Annu. Rev. Biochem.* 54:43–71.

Bohm, G., R. Muhr, and R. Jaenicke. 1992. Quantitative analysis of protein far UV circular dichroism spectra by neural networks. *Protein Eng.* 5:191–195.

Bian, S., and J. A. Cowan. 1998. Biological iron-sulfur cluster assembly. Detection of kinetic intermediates by time-resolved fluorescence spectroscopy. *J. Am. Chem. Soc.* 120:3532–3533.

Brahms, S., and J. Brahms. 1980. Determination of protein secondary structure in solution by vacuum ultraviolet circular dichroism. *J. Mol. Biol.* 138:149–178.

Chang, C. H., M. D. Ballinger, G. H. Reed, and P. A. Frey. 1996. Lysine 2,3-aminomutase: rapid mix-freeze-quench electron paramagnetic resonance studies establishing the kinetic competence of a substrate-based radical intermediate *Biochemistry.* 35:11081–11084.

Chattopadhyay, K., and S. Mazumdar. 2000. Structural and conformational stability of horseradish peroxidase: effect of temperature and pH. *Biochemistry.* 39:263–270.

Cowan, J. A and S. M. Lui. 1998. Structure–function correlations in high-potential iron proteins. *Adv. Inorg. Chem.* 45:313–350.

Cunningham, R. P., H. Asahara, J. F. Bank, C. P. Scholes, J. C. Salerno, K. Surerus, E. Munck, J. McCracken, J. Peisach, and M. H. Emptage. 1989. Endonuclease III is an iron-sulfur protein. *Biochemistry.* 28:4450–4455.

Dahms, T. E. S., and A. G. Szabo. 1997. Conformational heterogeneity in crystalline proteins: time-resolved fluorescence studies. *In* Fluorescence Spectroscopy. L. Brand and M. L. Johnson, editors. *Methods Enzymol.* 278:202–222.

Das, T. K., and S. Mazumdar. 1995a. Conformational substates of apoprotein of horseradish peroxidase in aqueous solution: a fluorescence dynamics study. *J. Phys. Chem.* 99:13283–13290.

Das, T. K., and S. Mazumdar. 1995b. pH-induced conformational perturbation in horseradish peroxidase. Picosecond tryptophan fluorescence studies on native and cyanide-modified enzymes. *Euro. J. Biochem.* 227:823–828.

Emptage, M. H. 1988. Aconitase; evolution of the active-site picture. *In* Metal Clusters in Proteins, Que, L., editor. ACS 372:343–371.

Godik, V. I., R. E. Blankenship, T. P. Causgrove, and N. Woodbury. 1993. Time-resolved tryptophan fluorescence in photosynthetic reaction centers from *Rhodobacter sphaeroides*. *FEBS Lett.* 321:229–232.

Haile, D. J., T. A. Roualt, J. B. Harford, M. C. Kennedy, G. A. Blondin, H. Beinert, and R. D. Klausner. 1992. Cellular regulation of the iron-responsive element binding protein: disassembly of the cubane iron-sulfur cluster results in high-affinity RNA binding. *Proc. Natl. Acad. Sci. U.S.A.* 89:11735–11739.

Hochkoeppler, A., P. Kofod, G. Ferro, and S. Ciurli. 1995a. Isolation, characterization, and functional role of the high-potential iron-sulfur protein (HiPIP) from *Rhodoferax fermentans*. *Arch. Biochem. Biophys.* 322:313–318.

Hochkoeppler, A., P. Kofod, and D. Zannoni. 1995b. HiPiP oxidoreductase activity in membranes from aerobically grown cells of the facultative phototroph *Rhodoferax fermentans*. *FEBS Lett.* 375:197–200.

Hochkoeppler, A., D. Zannoni, S. Ciurli, T. E. Meyer, M. A. Cusanovich, and G. Tollin. 1996. Kinetics of photo-induced electron transfer from high-potential iron-sulfur protein to the photosynthetic reaction center of the purple phototroph *Rhodoferax fermentans*. *Proc. Natl. Acad. Sci. U.S.A.* 93:6998–7002.

Hochstrasser, R. M., and D. K. Negus. 1984. Picosecond fluorescence decay of tryptophans in myoglobin. *Proc. Natl. Acad. Sci. U.S.A.* 81: 4399–4403.

Kennedy, M. C., L. Mende-Mueller, G. A. Blondin, and H. Beinert. 1992. Purification and characterization of cytosolic aconitase from beef liver and its relationship to the iron-responsive element binding protein. *Proc. Natl. Acad. Sci. U.S.A.* 89:11730–11734.

Kennel, S. J., R. G. Bartsch, and M. D. Kamen. 1972. Observations on light-induced oxidation reactions in the electron transport system of Chromatium *Biophys. J.* 12:882–896.

Kerefeld, C. A., C. Chan, M. Hirasawa, S. Kleis-SanFrancisco, T. O. Yeates, and D. B. Knaff. 1996. Isolation and characterization of soluble electron transfer proteins from *Chromatium purpuratum. Biochemistry.* 35:7812–7818.

Khan, K. K., S. Mazumdar, S. Modi, M. J. Sutcliffe, G. C. K. Roberts, and S. Mitra. 1997. Steady state and picosecond time-resolved fluorescence studies on recombinant *Bacillus megaterium* cytochrome P450 heme domain. *Euro. J. Biochem.* 244:361–370.

Külzer, R., T. Pils, R. Kappl, J. Hüttermann, and J. Knappe. 1998. Reconstitution and characterization of the polynuclear iron-sulfur cluster in pyruvate formate-lyase-activating enzyme: molecular properties of the holoenzyme form. *J. Biol. Chem.* 273:4897–4903.

Li, D., A. Agarwal, and J. A. Cowan. 1996. Evaluation of solvent accessibility to the $[Fe_4S_4]$ binding pocket in native and Tyr19 mutant high-potential iron proteins by ^1H-^{15}N HMQC and ^{19}F NMR experiments *Inorg. Chem.* 35:1121–1125.

Lovenberg, W., editor. 1973–1977. Role of iron-sulfur proteins in formate metabolism. *In* Iron-Sulfur Proteins. Vol. 1–3, Academic Press,.

Michaels, M. L., L. Pham, Y. Nghiem, C. Cruz, and J. H. Miller. 1990. MutY, an adenine glycosylase active on G-A mispairs, has homology to endonuclease III. *Nucleic Acids Res.* 18:3841–3845.

Natarajan, K., and J. A. Cowan. 1997. Identification of a key intermediate of relevance to iron-sulphur cluster biosynthesis. Mechanism of cluster assembly and implications for protein folding. *J. Am. Chem. Soc.* 119: 4082–4083.

Parisini, E., F. Capozzi, P. Lubini, V. Lamzin, C. Luchinat, and G. M. Sheldrick. 1999. *Ab initio* solution and refinement of two high potential iron protein structures at atomic resolution. *Acta Crystallogr. D.* 55: 1773–1784.

Prince, R. C., and M. J. Grossman. 1993. Novel iron-sulfur clusters. *Trends Biochem. Sci.* 18:153–159.

Przysiecki, C. T., T. E. Meyer, and M. A. Cusanovich. 1985. Circular dichroism and redox properties of high redox potential ferredoxins. *Biochemistry.* 24:2542–2549.

Robbins, D. J., M. R. Deibel, Jr., and M. D. Barkley. 1985. Tryptophan fluorescence of terminal deoxynucleotidyl transferase: effects of quenchers on time-resolved emission spectra *Biochemistry.* 24: 7250–7257.

Roulat, T. A., C. D. Stout, S. Kaptain, J. B. Harford, and R. D. Klausner. 1991. Structural relationship between an iron-regulated RNA-binding protein (IRE-BP) and aconitase: functional implications. *Cell.* 64: 881–883.

Spiro, T. G., J. Hare, V. Yachandra, A. Gewirth, M. K. Johnson, and E. Remsen. 1982. Resonance Raman spectra of iron-sulfur proteins and analogs. *In* Iron-Sulfur Proteins. Volume 4. T. G. Spiro, editor. John Wiley & Sons Inc., New York.

Switzer, R. L. 1989. Non-redox roles for iron-sulfur clusters in enzymes. *Biofactors.* 2:77–86.